Journal of Catalysis xxx (2015) xxx–xxx

Contents lists available at ScienceDirect

Journal of Catalysis

journal homepage: www.elsevier.com/locate/jcat

Post-synthesis Snβ: An exploration of synthesis parameters and catalysis

Jan Dijkmans [a], Jan Demol [a], Kristof Houthoofd [a], Shuigen Huang [b], Yiannis Pontikes [b], Bert Sels [a,*]

[a] *Center for Surface Science and Catalysis, KU Leuven, Kasteelpark Arenberg 23, 3001 Heverlee, Belgium*
[b] *Department of Materials Engineering, KU Leuven, Kasteelpark Arenberg 44, 3001 Heverlee, Belgium*

ARTICLE INFO

Article history:
Received 6 April 2015
Revised 23 June 2015
Accepted 29 June 2015
Available online xxxx

Keywords:
Heterogeneous catalysis
Lewis acid catalysis
Sn-beta
Post-synthesis procedures
Synthesis parameters
Adsorption process

ABSTRACT

Snβ is probably one of the best water tolerating heterogeneous Lewis acids for liquid phase catalysis. Instead of applying the usual lengthy hydrothermal synthesis to prepare Snβ, this contribution uses a more hands-on two-step synthesis method, involving the grafting of Sn precursors in isopropanol under reflux conditions on a commercial β zeolite that was dealuminated in acid. Among several reference synthesis procedures, this Sn introduction method resulted in active Sn catalytic sites. Taking advantage of this practical method, several synthesis parameters were explored and their impact on the catalytic activity in four different Lewis acid catalyzed reactions is discussed. The adsorption isotherm of Sn^{IV} in isopropanol over a broad range of Sn salt concentrations at reflux temperature is presented and discussed in relation with FTIR spectroscopy, UV–vis absorption characteristics and the porosity of the materials. The study reveals a selective Sn uptake, up to 2 wt% Sn loading, into silanol nests of the dealuminated precursor, forming a diversity of mononuclear Sn^{IV}. Higher Sn loadings result in less active Sn (hydrous) extraframework oxide phases, which also cause partial blockage of the zeolite micropores. Depending on the reaction type under study, space time yield may increase with increasing Sn loading, but the activity per Sn is always lower. Therefore it is concluded that a preferred synthesis should form high contents of isolated Sn active sites, especially for sugar isomerization and intermolecular Meerwein–Ponndorf–Verley, while the other reaction types like Baeyer–Villiger is also sufficiently catalyzed by the small Sn oxide clusters, albeit less actively.

1. Introduction

Sn-containing silica materials are widely studied in catalysis owing to their Lewis acid properties [1,2]. Tetrahedral Sn is able to expand its coordination with two extra ligands, forming an octahedral configuration [3,4]. Such expansion of coordination is useful for its interaction with organic reagents in a catalytic cycle. Formation of stable octahedral Sn sites, like in the framework of SnO_2, prevents such coordinative interaction rendering such materials catalytically inactive [5]. Therefore, homogeneous [6–12] and heterogeneous Sn-species with varying Sn geometry have been subject of many catalytic studies. The heterogeneous catalysts span from amorphous [13], over mesoporous [14–24] to highly crystalline zeolitic silica [1,2,25–29]. Among them, Snβ type zeolites show the highest catalytic activity, provided that not too large crystals or too bulky substrates are used [18,30,31]. According to literature, Snβ contains (in dried state) isolated and tetrahedrally coordinated Sn^{IV}, built into the framework [32]. The catalyst has been used successfully in several chemical transformations, including hydrogen-shift, oxidation and carbon–carbon coupling reactions [25,30,33,34]. Though there is a general agreement on the presence of Lewis acidity because of Sn incorporation, the exact nature of the Sn active catalytic site is under debate. So far, two different Sn^{IV} active sites have been revealed showing a common 4-O inner-sphere complexation [4]: a perfect framework substitution leading to $Sn(OSi)_4$, also denoted as ‘closed’ site and a partly hydrated Sn species, formally written as $Sn(OSi)_3(OH)$ and termed ‘open’ Sn sites [3,35]. A schematic representation of both sites is shown in Scheme 1. Multiple reports currently discuss the importance (or not) of SnOH and nearby SiOH groups for the catalytic properties [4,36,37]. Aside from the framework Sn-species, catalytic activity has also been ascribed to small extra-framework (EFW) oxidic Sn particles within the hydrophobic pores of the zeolite, whereas large Sn oxide particles on the crystal surface do not show this activity [5].

Snβ is usually synthesized by a traditional hydrothermal synthesis, that is above the water boiling point, in a closed vessel, reaching super-atmospheric pressure (Scheme 2, top pathway) [25,32]. During the synthesis process, Sn is gradually incorporated into the beta zeolite framework. Unfortunately, nucleation of Snβ from Sn-containing gels is difficult. To facilitate the crystallization

---

* Corresponding author.
E-mail address: bert.sels@biw.kuleuven.be (B. Sels).

http://dx.doi.org/10.1016/j.jcat.2015.06.023
0021-9517/© 2015 Elsevier Inc. All rights reserved.

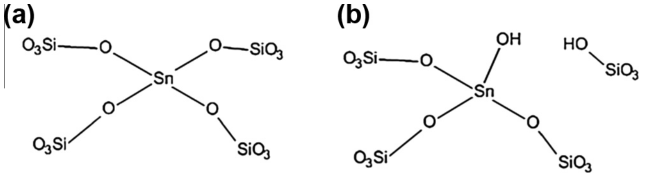

Scheme 1. Schematic representation of a (a) closed tetrahedral Sn-site and (b) an open tetrahedral Sn-site.

process addition of seed crystals is often used [38]. In spite of successful synthesis of Snβ, long synthesis times and hazardous mineralizing agents like HF or NH_4F are indispensable. More practical synthesis methods are therefore proposed. Modification of seeding procedures result in increased rate of crystallization, while other syntheses use steam to convert dry Sn gels into Snβ materials [39,40]. Unfortunately, these methods maintain the need for F-ions as mineralizing agents.

A different approach is followed in the so-called secondary (or post-) synthesis procedures. Instead of bottom-up synthesis, pre-formed zeolites like beta are doped with Sn (top-down approach, Scheme 2 bottom pathway). Usually, the parent zeolites are subjected to an acid treatment to remove (part of) framework Al (or Si or B), leading to dealuminated zeolites rich in silanol nests [41–44]. These silanol groups function as anchoring points for the Sn precursor. Among the top-down synthesis procedures, there is a large variety of ways to introduce Sn. A solid-gas reaction with gaseous $SnCl_4$ at elevated temperatures for instance results in a 6 wt% Snβ containing substantial amounts of framework Sn active sites but also catalytically inactive EFW SnO_2 [45,46]. A practical alternative, first introduced by the Hermans' group, describes a solid-state mixing method of the dealuminated beta zeolite with Sn^{2+}acetate, followed by calcination. They showed the synthesis of Snβ with extremely high Sn content, up to 10 wt%, avoiding substantial content of EFW SnO_2 [47]. In a similar procedure, use of dimethyltin dichloride resulted in a 3.8 wt% of Snβ [48]. Finally, an adsorption process of $SnCl_4$ in dried isopropanol under reflux conditions, was recently communicated by our group, leading to an active 1.6 wt% Snβ [49,50].

The notion of turnover frequency (TOF) is used as a measure of the intrinsic activity of a catalytic site. In Sn-catalyzed materials too, efforts are reported to achieve maximal TOF values [4,49,51]. Though comparison between different reports is not always straightforward, as several reaction types are investigated at different reaction conditions. In addition, use of TOF values implies the absence of any mass transfer rate limitation, causing underestimation of the true potential of the Sn sites and the determination of the concentration of the active site, provided the identity of the latter is known [14,31]. Also the heterogeneity of Sn sites makes the determination of genuine turn-over frequencies rather challenging. Alternatively, a property known as the space-time yield (STY) is often used to evaluate the practical potential of a catalytic material, as not the activity per site but per catalyst weight is involved. Careful inspection of Snβ literature indeed indicates that a high Sn content is mostly not a guarantee for a high STY, as often TOF gradually decreases with increasing Sn, even when the authors correctly identified the exclusive presence of isolated tetrahedral Sn^{IV} [46,49,51].

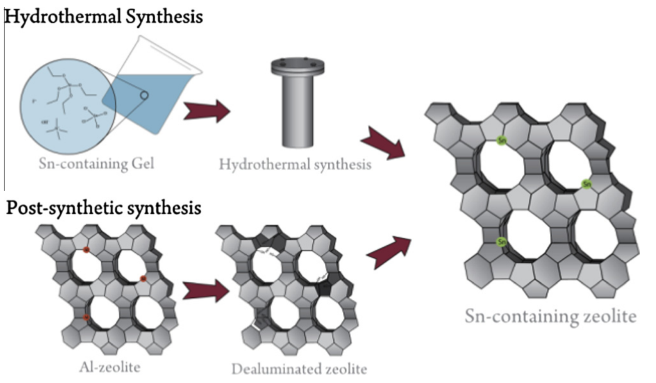

Scheme 2. Schematic representation of synthesis pathways of Sn-containing zeolites. The top pathway shows the traditional (bottom-up) hydrothermal synthesis; a Sn-containing gel in an autoclave is placed in an oven for a period of time and the molecular building blocks assemble to form the Sn-containing zeolite at high temperature and pressure. The bottom pathway shows the post-synthetic or secondary synthesis. An Al-containing zeolite is dealuminated during an acid treatment or steaming operation. The dealuminated zeolite is then modified with a Sn precursor.

This work evaluates variously prepared Snβ zeolites for four different reaction types and their catalytic data, expressed in both TOF and STY. The selected reactions are glucose isomerization (ISOM) to fructose, Meerwein–Ponndorf–Verley (MPV) of cyclohexanone with 2-butanol to cyclohexanol, Baeyer–Villiger (BV) oxidation of cyclohexanone to caprolactone and a multi-step conversion (via dehydration – MPV (DH/MPV)) of 1,3-dihydroxyacetone in ethanol to ethyl lactate (Scheme 3). The products of these reactions have applications as sweetener (fructose) or polymer building blocks [52,53,54,55]. First, a set of reported post-synthetic procedures is evaluated and compared, and the best method is used to exploit the effect of numerous synthetic parameters such as Sn precursor type and concentration and water content on the catalytic properties. Interestingly, the results will show that the best parameter set differs for some of the tested reactions, pointing to a diversity of Sn sites and different Sn active site requirements. Catalytic data are finally linked with Sn active site characteristics, as provided by electronic and vibrational spectroscopy, and with pore blockage phenomena.

2. Experimental

2.1. Material synthesis

Commercial β zeolite (CP814e, Zeolyst International, SiO_2/Al_2O_3 = 25) was dealuminated by stirring the zeolite powder

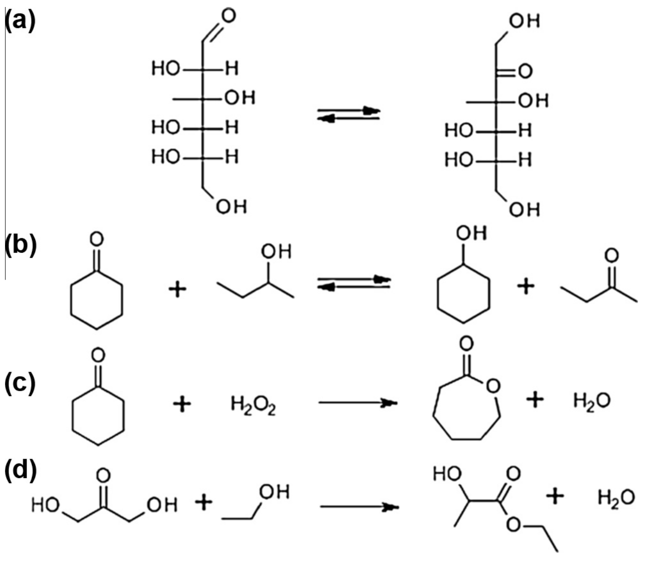

Scheme 3. Overview of the reactions studied. (a) Isomerization of glucose to fructose; (b) Meerwein–Ponndorf–Verley reaction of cyclohexanone and 2-butanol forming cyclohexanol and 2-butanone; (c) Baeyer Villiger oxidation of cyclohexanone with hydrogen peroxide yielding ε-caprolactone and water; (d) transformation of 1,3-dihydroxyacetone in ethanol to ethyl lactate.

Please cite this article in press as: J. Dijkmans et al., Post-synthesis Snβ: An exploration of synthesis parameters and catalysis, J. Catal. (2015), http://dx.doi.org/10.1016/j.jcat.2015.06.023

overnight in an aqueous HNO_3 solution (55 ml/g of zeolite, overnight at 353 K), an acid concentration of 7.2 M was used. Afterward the solids were filtered, washed with water and dried at 333 K. All of the post-synthesis procedures were preceded by an activation of the dealuminated zeolite at 423 K to remove any physisorbed water, followed by a calcination step in air at 823 K. Samples made by an impregnation method (IMP) with $SnCl_4 \cdot 5H_2O$, containing 2 wt% of Sn w.r.t. dry zeolite powder, were slurried in dry isopropanol (5 ml of alcohol per gram of zeolite powder). The solvent was slowly evaporated at 323 K under vigorous stirring, causing Sn precipitation onto the zeolite [56]. For samples made by a chemical vapor deposition (CVD), the procedure described by de Correa et al. was used [24]. The required amounts of $SnCl_4$ and dealuminated beta zeolite were placed into a Teflon-lined stainless steel autoclave, that was heated at 373 K for 8 h. Materials made by a solid mixing procedure (Solid-MIX), underwent manual grinding for several minutes, using a mixture of dealuminated zeolite and $SnCl_4 \cdot 5H_2O$ powder in the required amounts [56]. Grafting of $SnCl_4$ onto the dealuminated beta zeolite was tested in two different solvents. For the H_2O-graft, a procedure described by Zhang et al. was followed [57]. The second solvent in the grafting procedure was dried isopropanol (IPA-graft), using a method described by Wagner et al. for grafting Sn onto mesoporous carrier materials [58]. The dealuminated zeolite was added to $SnCl_4 \cdot 5H_2O$ (27 mmol/g of zeolite) in water or dry isopropanol (100 ml/g of zeolite) and placed in a reflux setup under N_2 atmosphere. After 7 h, the mixture was filtered in air, rinsed with water or dried isopropanol and dried at 333 K. When varying the Sn-precursor, equimolar amounts of the new precursor were used. All other synthesis parameters were kept constant. Metallic Sn^0 powder was converted *in situ* to a Sn-salt by adding a 4.0 M HCl in 1,4-dioxane-solution (8 moles of HCl per mole of Sn^0) to the isopropanol reflux solution. As the intended catalytic material is investigated as an alternative for the hydrothermally (HT) synthesized Snβ, this material was synthesized using a procedure described in literature [59]. The hydrothermally synthesized and post-synthetically treated beta zeolite crystals used in this work have dimensions, as measured with SEM of 1000–1500 and 10–30 nm, respectively [49]. This is far below the limit at which pore diffusion limitations was shown to take place (>7 μm [31]). Therefore the catalytic reaction rates are assumed to be diffusion free and only determined by the chemical transformations.

2.2. Catalytic tests

Catalytic tests were performed in magnetically stirred and closed glass reactors of 10 ml, which were placed in a copper block. Temperature control is carried out in a reference glass reactor with solvent. For isomerization reactions, 100 mg of catalyst was added to 5 ml of a 10 wt% aqueous glucose solution. The reactions were performed at 383 K. For Baeyer–Villiger reactions, 1.11 mmol of ketone was added to 50 mg of catalyst in 5 ml of dioxane. 50 wt% aqueous H_2O_2 solution was added in a molar H_2O_2/ketone-ratio of 2. Ethylcyclohexane was used as the internal standard for chromatographic analysis. The reactions were performed at 363 K. Meerwein–Ponndorf–Verley reactions were performed at 373 K. 15 mg of catalyst was added to a 2-butanol solution containing 1 mmol of ketone, the solvent was used in a 2-butanol/ketone ratio of 50. 1,4-Dioxane was used as an internal standard. For the conversion of dihydroxyacetone to ethyl lactate, 1 mmol of substrate was dissolved in 5 ml of ethanol, 1,4-dioxane was used as internal standard. 75 mg of catalyst was used. The reaction was performed at 363 K. For each reaction, aliquots of the sample were taken at regular time intervals through a rubber septum and were quantitatively analyzed with an Agilent 6850 GC, equipped with a HP-1 column and FID detector. For non-volatile products, an Agilent 1200 series HPLC equipped with Metacarb 67C column and RI detector was used. Identification of the products was based on retention time analysis and confirmed by GC–MS (Agilent 6890 GC with HP5-MS column and Agilent 5973 Mass Selective Detector). TOFs were calculated as $\text{mole}_{\text{product}}\ \text{mole}_{\text{Sn}}^{-1}\ \text{h}^{-1}$, while STY was determined as $\text{g}_{\text{product}}\ \text{g}_{\text{catalyst}}^{-1}\ \text{h}^{-1}$.

2.3. Characterization techniques

The Sn-content of the materials was all determined by electron probe microanalyzer (EPMA) analysis conducted on a JEOL JXA-8530F field emission microprobe using WDS. Samples were embedded in a resin, and the surface was ground, polished and coated with carbon before measurement. The microprobe was operated at 10 kV with a probe current of 1.5 nA. The Sn $L_{\alpha 1}$-signal was detected using a PETH crystal and the Sn concentration was quantified with a cassiterite standard. ZAF was used for the matrix correction method. Absorption in the UV–vis region was recorded on an Agilent Cary 5000 spectrophotometer. Samples were placed in a quartz tube with window, and were dried at 823 K in a dry N_2-flown (unless stated otherwise) before measurement using a heating rate of 5 K/min. Samples were corrected with a calcined dealuminated beta zeolite to isolate Sn-related signals. FT-IR measurements of the silanol groups were performed on a Nicolet 6700 Spectrometer equipped with DTGS detector. The materials were pressed into self-supporting wafers and degassed at 673 K *in vacuo* before measurement at 423 K. The broad silanol signal was deconvoluted into the individual signals using OriginPro 8 software using fixed FWHM values for the signals between the materials. Lewis acid sites were probed with deuterated acetonitrile, cyclohexanone and pyridine as probe molecule. Deuterated acetonitrile was adsorbed at room temperature. The samples were exposed to 100 mbar of probe molecule for 10 min., afterward desorption *in vacuo* of the molecule was followed at the same temperature. For pyridine adsorption, the samples were subjected to 25 mbar of the probe until saturation at 323 K. Spectra were recorded at 423 K *in vacuo* after equilibration for 20 min. 0.89 cm μmol^{-1} was used as integrated molar extinction coefficient for calculation of Lewis acid density [60]. For cyclohexanone the samples were exposed to 6.5 mbar of probe molecule until saturation at room temperature. Spectra were recorded at different temperatures *in vacuo* after equilibration of 10 min. at each heating step. X-ray diffraction patterns were recorded on a STOE Stadi P diffractometer equipped with Cu $K\alpha_1$ source and IP-PSD detector. Before measurement, the samples were stored in a controlled humidity environment, *ie*. above an aqueous saturated NH_4Cl solution (79% humidity). ^{119}Sn MAS NMR spectra were recorded on a Bruker DSX400 spectrometer (B_0 = 9.4 T) operating at a NMR frequency of 149.21 MHz. Single-pulse excitation measurements with varying interscan delays between 5 and 40 s have been used. The samples were packed in 4 mm zirconia rotor; the spinning frequency of the rotor was 12,000 Hz. The chemical shift is referenced with respect to $Sn(CH_3)_4$. SnO_2 was used as a secondary standard; the chemical shift of its center band was set at −604.0 ppm [61]. N_2 sorption measurements were performed using a Micromeritics Instruments Tristar 3000 at 77 K. Samples were degassed under nitrogen flow at 527 K overnight prior to measurement. Pore volumes were calculated using the *t*-plot method.

3. Results and discussion

3.1. Catalytic exploration of various post-synthetic Snβ materials

The catalysts studied in this work are all synthesized according to (top down) post-synthesis routes. All procedures start with a

Please cite this article in press as: J. Dijkmans et al., Post-synthesis Snβ: An exploration of synthesis parameters and catalysis, J. Catal. (2015), http://dx.doi.org/10.1016/j.jcat.2015.06.023

commercial aluminum containing β zeolite (Zeolyst CP814E, $SiO_2/Al_2O_3 = 25$). Incorporation of Sn proceeds in two consecutive steps. First, the zeolite material is dealuminated by an acid treatment using a 7.2 M HNO_3 aqueous solution. Such dealumination of beta zeolites has been studied extensively in the past [41,42,62–65]. Though the BEA structure is conserved during this acid treatment, extensive removal of Al is observed, creating residual holes in the framework surrounded by silanol groups. In a second step, a Sn-containing precursor interacts with these silanol groups, forming a covalent Si—O—Sn bond introducing Sn in the zeolite framework (Scheme 2, bottom pathway) [49]. Several procedures to introduce Sn onto carrier materials have been described [16,24,47,48,56–58,66]. Inspired by them, we selected several synthesis procedures to achieve the most active catalytic material.

In total, six materials were synthesized. Five materials were made by using different Sn introduction methods and one reference material was synthesized using the traditional hydrothermal (HT) procedure [59]. The Sn introduction methods, which were used, are as follows: impregnation (IMP) [56], chemical vapor deposition (CVD) [16,24], solid mixing (Solid-MIX) [56] and grafting in water (H_2O-graft) [57] and dried isopropanol (IPA-graft) [58]).

Results of the elemental analysis of the synthesized materials are displayed in Table 1. All samples show Sn-contents ranging from 1 to 3 wt%, except for the material synthesized by grafting of $SnCl_4{\cdot}5H_2O$ in water, which showed an elevated Sn-content of 27.6 wt%. This sample colored yellow, whereas all other samples were white. EPMA analysis of this water-grafted sample clearly showed two distinct regions. The first was the zeolite with high amount of Sn (20 wt%), corresponding to a Si/Sn-ratio of 7.3. A second region was identified as SnO_2 (see Fig. S1). The use of water as a solvent in the grafting procedure thus leads to formation of a large SnO_2-phase, a catalytically inactive oxide. EPMA of the other synthesis procedures shows a homogeneous phase of zeolite particles, containing Sn according to the aforementioned elemental compositions.

Data of the catalytic tests with the five catalysts for the four reactions are collected in Table 1. A tentative catalyst ranking based on the average activity per Sn site shows the following order: for ISOM: HT > IPA-graft > CVD = IMP > H_2O-graft > Solid-MIX; for MPV: IPA-graft > HT > IMP > Solid-MIX > CVD > H_2O-graft; for BV: IPA-graft = Solid-MIX > HT > CVD = IMP > H_2O-graft; and for DH/MPV: IPA-graft > IMP > HT > CVD > Solid-MIX > H_2O-graft.

Clearly, the order of preferred Sn active sites is different for each reaction type, pointing to different Sn active site requirements. As expected, the highly Sn-loaded H_2O-graft performs inferior in all reactions, due to the presence of inert SnO_2. In general, IPA-graft performs best for most reaction types. For instance, TOF values of 96, 49 and 103 h^{-1} were measured for MPV, BV and DH/MPV, respectively (Entry 5). Only for ISOM the Sn active sites of the original HT are preferred, despite having the largest crystals of the five materials tested [49,50]. A high TOF value of 306 h^{-1} was obtained with HT, whereas the second best IPA-graft has a TOF of 133 h^{-1} (compare Entries 5 and 6). Surprisingly high Sn activity in BV is observed with the Solid-MIX, almost equally comparable with the IPA-graft (47 and 49 h^{-1}, respectively), whereas this catalyst shows only moderate Sn activity for the other reaction types. Similarly, the Sn active sites in IMP are not very active for most reactions except for DH/MPV. Here, the Sn active sites perform nearly as good as those in IPA-graft, showing TOFs of 87 and 103 h^{-1}, respectively (compare Entries 1 and 5).

The conclusions are slightly different by comparing STYs. The following activity order can be extracted: for ISOM, HT > IPA-graft > CVD = IMP > H_2O-graft > Solid-MIX; for MPV, IPA-graft > HT = IMP > CVD > Solid-MIX > H_2O-graft; for BV, IPA-graft > CVD > Solid-MIX > HT > IMP > H_2O-graft; and for DH/MPV, IMP > IPA-graft > HT = CVD > Solid-MIX > H_2O-graft. As before, IPA-graft performs very good in most reaction types. Most notable is probably the successful use of IMP for DH/MPV catalysis, showing very high STY of about 1737 h^{-1} and the disappointing results with HT in catalyzing this reaction (Entry 1 *vs.* 6). The changes in the activity order between TOF and STY are due to differences in Sn content. Literature data and results in this work (*vide infra*) reveal that a simple increase of Sn not necessarily means a linear increase of STY, pointing to the formation of various Sn species with different catalytic activity. For ISOM, it was demonstrated that active Sn sites in Snβ synthesized by grafting or solid mixing procedures provide high activity sites at low Sn-content. Maximal STY however was often reached at moderate Sn-content [49,51]. A similar conclusion may be extracted from reported data for a gaseous grafting procedure; a constant STY value was observed despite a rising Sn-content, as confirmed by a decreased TOF [46].

The initial screening of the different Sn-incorporation procedures thus demonstrates that the synthesis of catalytically active materials using straightforward and practical post-synthesis procedures is possible, in line with other literature reports [43–49]. Depending on the reaction type, however, different optimal active sites are found and consequently, variation in synthesis method and parallel characterization is advisable. As the highest activity for most reactions was reached with IPA-graft, this synthesis method will be applied in the continuation of this work, describing the impact on the catalytic activity of various synthesis parameters, like Sn precursor type, Sn loading and water content.

3.2. Effect of precursor concentration

First, the effect of varying $SnCl_4{\cdot}5H_2O$ concentrations on the Sn loading and Sn oxide speciation of the final material was studied. The adsorption isotherm at reflux temperature, displayed in Fig. 1a, show two different Sn adsorption sites on the dealuminated beta zeolite, one at low (site A) and one at high Sn loading (site B). The isotherm shows a clear Sn adsorption at low $SnCl_4{\cdot}5H_2O$ concentrations with moderate affinity, corresponding to an uptake efficiency of 8.3 μmol Sn per soluble mmol Sn per gram of dealuminated zeolite. The adsorption site is saturated at 0.3 M equilibrium Sn concentration, corresponding to a 1.6 wt% or 0.13 mmol g^{-1} Sn

Table 1
Comparison of the Sn-content and catalytic performance in the ISOM, MPV, BV and HS reactions catalyzed with materials synthesized according to different synthesis procedures.

Entry	Synthesis method	Sn-content	ISOM		MPV		BV		DH/MPV	
			STY	TOF	STY	TOF	STY	TOF	STY	TOF
		wt%	h^{-1} (×1000)	h^{-1}	h^{-1} (×1000)	h^{-1}	h^{-1} (×1000)	h^{-1}	h^{-1} (×1000)	h^{-1}
1	IMP	2	702	23	758	45	402	21	1737	87
2	CVD	2.9	722	16	350	14	606	22	1069	37
3	Solid-MIX	1	0	–	246	29	462	47	269	27
4	H_2O-graft	27.6	280	0.7	57	0.3	156	0.6	69	0.3
5	IPA-graft	1.6	3640	152	1277	96	742	49	1621	103
6	HT	1.3	5880	306	824	78	448	37	1131	72

Please cite this article in press as: J. Dijkmans et al., Post-synthesis Snβ: An exploration of synthesis parameters and catalysis, J. Catal. (2015), http://dx.doi.org/10.1016/j.jcat.2015.06.023

loading. This value is unexpectedly low taking into account that about 0.9 mmol g^{-1} Al is removed. This low uptake, which is currently difficult to rationalize, could be indicative of a T site-specific adsorption process in the dealuminated Beta zeolite. After site A saturation, a linear increase of Sn content is set in with increasing $SnCl_4{\cdot}5H_2O$ equilibrium concentration above 0.30 M. The affinity of the site B for Sn, corresponding to 5.2 μmol adsorbed Sn per mmol Sn in solution per gram, is somewhat lower than that of site A. Absence of a saturation point is noticed at least up to 8 wt% Sn loading, indicative of a non-specific adsorption mechanism.

More proof of a dual $SnCl_4$ adsorption mechanism is given by inspection of the FTIR spectra in the silanol vibrational range. Two silanol species were therefore monitored after varying Sn content uptakes and sample calcination; the internal silanols, formed by the dealumination procedure, show a characteristic absorption around 3730 cm^{-1}, while external silanols at crystal surfaces and defects are visible at 3740 cm^{-1} [41]. The absorption area of both silanol species, relative to these in a Sn-free dealuminated material is plotted against the Sn-content in Fig. 1c. Clearly, internal silanol groups are consumed up to about 2 wt% Sn content, suggesting that these silanols are involved in site A adsorption. As higher Sn uptake occurs without further consuming silanols, site B adsorption is not associated with the silanol nests, but rather implies a structure independent extraframework (EFW) species. The external silanols appear unreactive during the Sn grafting procedure.

As the FTIR analysis suggests a different identity of Sn in the two adsorption sites, a similar detailed study was carried out with diffuse reflectance UV–vis spectroscopy (Fig. 1b). DR UV–vis on dried samples was used to investigate the electronic properties of the adsorbed Sn species, through the charge transfer absorption of Sn—O. Absorption in the low energy UV range (280–350 nm) is indicative of an octahedral coordination in Sn^{IV} species, often of polymeric nature like in bulk SnO_2. Isolated tetrahedrally coordinated Sn^{IV} absorbs high energy UV light at 200 nm [5]. The intensity at 200 nm was used as indicator of isolated Sn sites, whereas the intensity at 255 nm shows the presence of oligomeric, assumedly tetrahedrally coordinated, Sn oxide species. The intensities were plot against the Sn loading and superimposed onto Fig. 1a.

Except for the sample free of Sn, all catalysts show clear absorbance at 200 nm and this signal rises linearly with the adsorption of Sn on the internal silanols (site A). This site matches with the

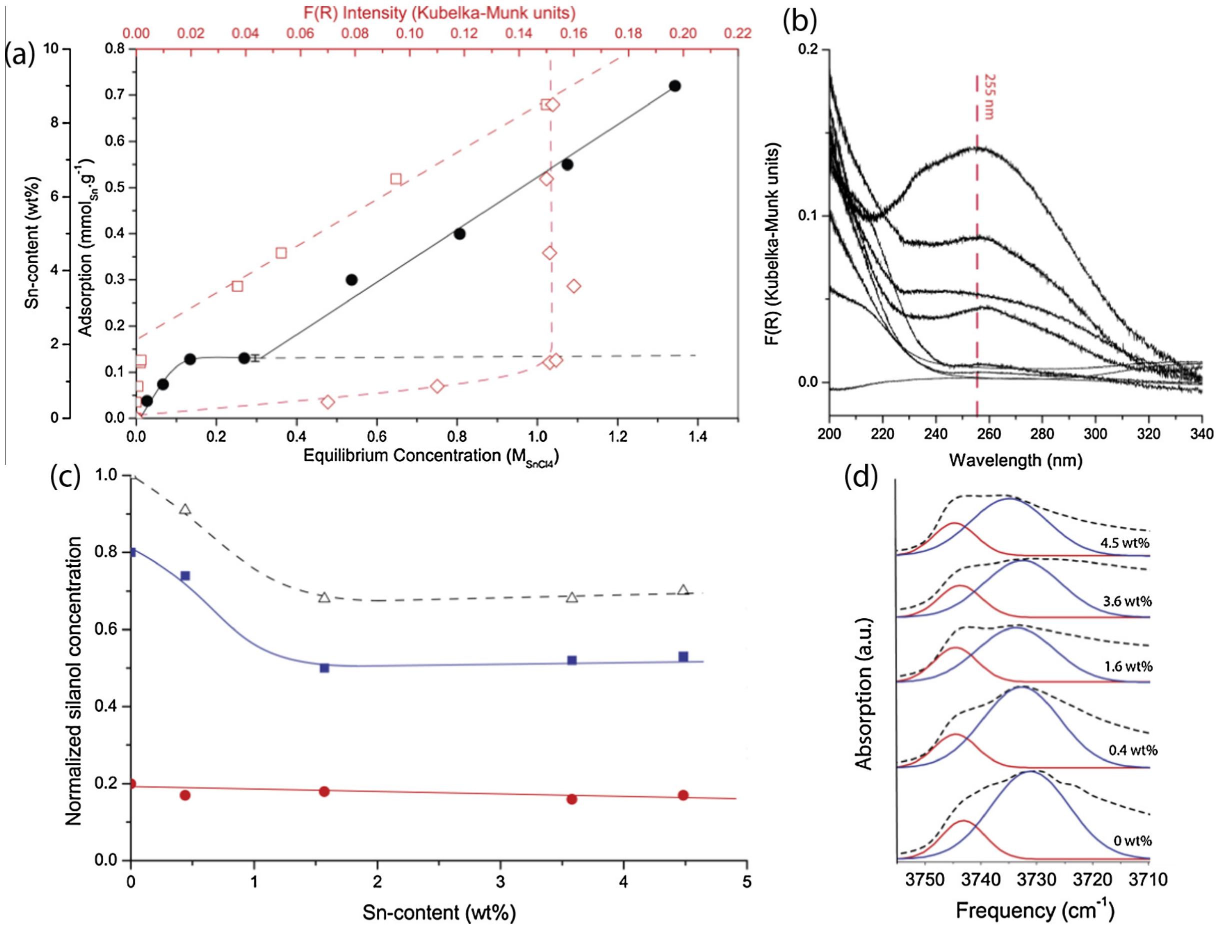

Fig. 1. (a) Left and bottom axis, ●: equilibrium concentration of $SnCl_4{\cdot}5H_2O$ used in the grafting procedure and the Sn-content of the final Sn-grafted materials. The lines are guide to the eyes. A standard deviation error bar for the Sn-content of samples grafted with 0.27 M $SnCl_4{\cdot}5H_2O$ (based on 5 separate samples) is shown next to the data point. Left and top red axis, red hollow data points: Intensity of the 200 (◊) and 255 nm (□) signal as recorded with UV–vis for dried samples with varying Sn-content. The intersection of the red line (□) and y-axis, around 2 wt%, indicates the maximal tetrahedrally coordinated isolated Sn-content possible without substantial presence of other Sn oxide species. (b) UV spectra with varying Sn content (increasing Sn-content from bottom to top. The spectra are corrected with a calcined dealuminated zeolite to isolate the Sn-related signals. (c) Normalized concentration of internal (▪) and external (●) silanol groups in function of the Sn-content of the materials. The sum of both species (Δ) is shown with dotted line. Lines are guide to the eye. The data were obtained by deconvolution of the FTIR signal for the 3730 (internal) and 3740 (external) cm^{-1} signals. Signal was scaled to weight. d. FTIR spectra of samples with varying Sn content with the deconvolution of the signals for internal and external silanol groups. The red line indicates the 3740 cm^{-1} signal for external silanols, the blue line shows the 3730 cm^{-1} signal for internal silanol and the dotted black line shows the recorded signal. The broad shoulder at lower frequencies is caused by hydrogen bonded silanol groups, the fitting being omitted in the graph for reasons of clarity. (For interpretation of the references to color in this figure legend, the reader is referred to the web version of this article.)

Please cite this article in press as: J. Dijkmans et al., Post-synthesis Snβ: An exploration of synthesis parameters and catalysis, J. Catal. (2015), http://dx.doi.org/10.1016/j.jcat.2015.06.023

formation of the tetrahedral Sn sites, pointing out that about 2 wt% of Sn can be selectively accommodated in this particular site. Further increase of the Sn loading is no longer accompanied with an increase of the 200 nm signal. Instead, a 255 nm feature becomes more dominant with increasing Sn loadings above 2 wt%. Though its exact molecular nature is unknown, its low energy absorption suggests an octahedral mono- or oligo-meric or a tetrahedral oligomeric Sn oxide speciation, which agrees with the EFW location, suggested by the IR analysis [5,67,68]. Sizes of SnO_2 may be obtained from the wavelength at maximum absorption, showing a shift to higher wavelengths for increasing oxide particle size [5,69]. As no shift in the absorption maximum is observed, size of the oxides particles is assumed to be constant, and the higher absorption intensity is caused by an increased concentration.

Further information about the identity of the 255 nm signal was obtained with X-ray diffraction. The patterns of three grafted samples, having resp. 1.6, 4.5 and 8.5 wt% Sn, are illustrated in Fig. 2(c–e) together with the Sn-free dealuminated beta (b) and a SnO_2 reference (a). The characteristic d_{302} reflection ($2\theta = 22.4°$) of the BEA topology is visible in all samples, while d_{101} and d_{211} reflections ($2\theta = 33.8°$ and $51.7°$ resp.) of bulk SnO_2 show only weak intensities for the highest Sn loading (8.5 wt%). As a 0.5 wt% detection limit was established for the presence of bulk SnO_2 with X-ray analysis [50], the present Sn oxide phase is likely less crystalline in nature except for highest Sn-loading.

The influence of the two types of Sn sites on the catalytic properties (STY and TOF) is evaluated for the four model reactions in function of the Sn loading (Fig. 3 and Table S1) In all reaction types, the highest TOFs are found for samples with low Sn content.

Though UV–vis absorption demonstrated a single active site of tetrahedral Sn below 2 wt% Sn loading, maximum turnovers per Sn were always observed at the lowest Sn content (0.5 wt%). This observation is in line with reported data for various post-synthetic synthesis procedures [46,49,51]. Therefore, the 200 nm absorption, represented by the Sn adsorbed in site A, likely represents a diversity of catalytic Sn sites with different activities. Such heterogeneity in the catalytic properties of the 200 nm absorbing Sn-species may be due to the varying site specifications, but also its location and thus its steric demand in the zeolite framework may cause dissimilarities in the kinetic parameters. Numerous literature examples describe changed catalytic properties in enzymatic, homogeneous and heterogeneous catalysts due to small structural alterations [35,70–73].

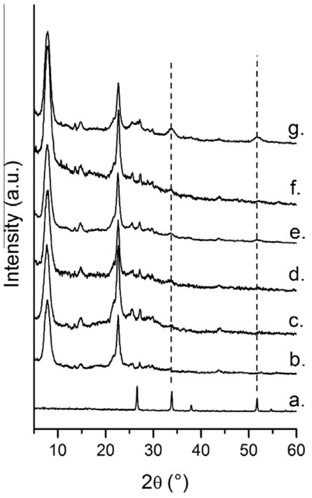

Fig. 2. X-ray diffraction pattern of (a) SnO_2, (b) Dealuminated Beta zeolite and (c) 1.6 wt% Sn (0.27 M $SnCl_4{\cdot}5H_2O$, $H_2O{:}Sn = 5$), (d) 4.5 wt% Sn (0.81 M $SnCl_4{\cdot}5H_2O$, $H_2O{:}Sn = 5$), (e) 8.5 wt% Sn (1.35 M $SnCl_4{\cdot}5H_2O$, $H_2O{:}Sn = 5$), (f) 7.1 wt% Sn (0.27 M $SnCl_4{\cdot}5H_2O$, $H_2O{:}Sn = 12$) and (g) 11.3 wt% (0.27 M $SnCl_4{\cdot}5H_2O$, $H_2O{:}Sn = 31$) grafted zeolite. The d_{101} and d_{211} SnO_2 reflections are indicated with a vertical dotted line.

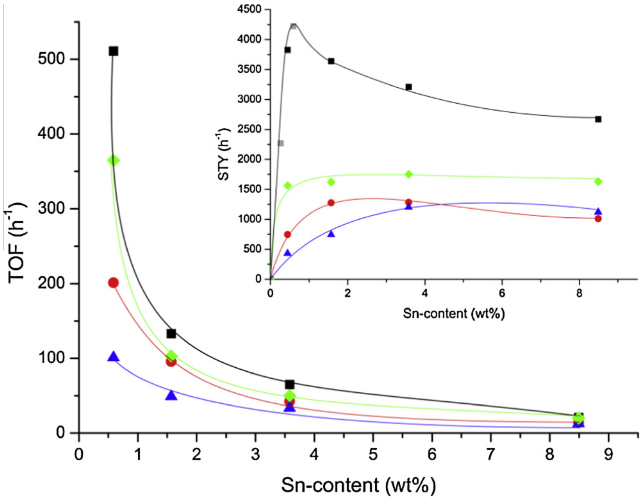

Fig. 3. Plot of TOF and STY (×1000, inset) in function of Sn-content for the ISOM (black squares), MPV (red circles), BV (blue triangles) and DH/MPV (green diamonds) reaction. For the STY-plot of the ISOM reaction, extra data points (gray) from Ref. [49] are added for clarity. Sn-content was varied by varying the $SnCl_4{\cdot}5H_2O$ concentration in the IPA grafting liquid. The lines are guides to the eye. (For interpretation of the references to color in this figure legend, the reader is referred to the web version of this article.)

The STY of the four reactions in function of the Sn loading is displayed in the insert of Fig. 3. As STY values initially increases, the lower activity per Sn (TOF) is largely compensated by the amount of Sn. However, the optimal Sn loading to achieve maximum STY depends on the reaction type. The catalyst containing about 1 wt% Sn is preferred for ISOM, whereas higher Sn loadings of 2 and 4 wt% are required for high STY in MPV and BV, respectively.

Higher Sn loadings cause a decrease in catalytic activity. Three reasons may be invoked to explain this phenomenon: formation of EFW SnO_2 hides Sn atoms into its structure, Lewis acid sites of the EFW are catalytically less active due to site-specific requirements, or EFW particles block micropores. Probing of Lewis acid sites with pyridine is a useful method to evaluate Sn site accessibility. The data are presented in Fig. 4 and Table S2. A constant Lewis acid-to-Sn molar ratio of 0.7 was monitored for Sn loadings below 2 wt%, corresponding to Sn in site A. Though a ratio of 1 was expected, deviation is explained by either the presence of some weaker Lewis acid sites, not probed by the method, or more likely by the uncertainty of the molar extinction coefficient in the quantification, as multiple values are reported [50,60,74–76]. Higher Sn-loadings show more Lewis acid sites, likely due to additional Lewis acidity of the EFW species, but the increase deviates from linearity with the Sn content as lower Lewis acid-to-Sn molar ratios were measured: for instance, 0.5 and 0.3 for 3.6 and 4.5 wt% Sn samples, respectively. Pore blockage (partially) explains this deviation as a systematic drop in micropore volume was noticed for the highly loaded Sn samples, in concert with the drop in acid-to-Sn molar ratio (Fig. 4). For instance, $0.16\ mL\ g^{-1}$ pore volume was measured for the 1.6 wt% loading, whereas this value drops to $0.12\ mL\ g^{-1}$ for the 4.5 wt% sample. However, as normalizing the number of Lewis acid sites for total micropore volume is insufficient to provide a linear correlation with the Sn content (Fig. S2), inaccessibility of Sn atoms in the inner parts of the EFW particles should also be invoked to explain the lower acid-to-Sn molar ratios for the highly loaded samples.

Please cite this article in press as: J. Dijkmans et al., Post-synthesis Snβ: An exploration of synthesis parameters and catalysis, J. Catal. (2015), http://dx.doi.org/10.1016/j.jcat.2015.06.023

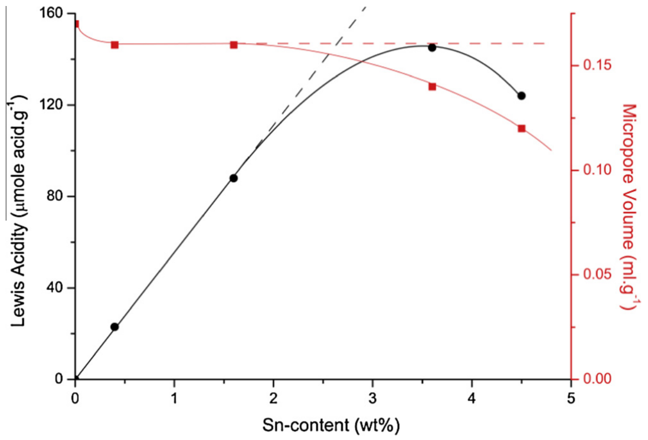

Fig. 4. Lewis acidity (left axis, ●) and the micropore volume (right axis, 🟥) in function of the Sn-content of the materials. Lines are guide to the eye. Black dotted line indicates a linear increase in acidity, red dotted line indicates a stable micropore volume.

Similar as for the Lewis acidity of the materials, normalizing STY for total micropore volume (Fig. S3) provides insight into the trends of changing STY's with high Sn loadings. For ISOM and MPV, a plateau in the normalized STY is reached at loadings of respectively 0.4 and 2 wt%, indicating that the observed decrease in STY, as presented in Fig. 4, is directly attributed to inaccessibility of Sn sites by pore blockage. BV, and to lesser extent DH/MPV, shows a linear increase for the normalized STY at Sn-contents above 0.4 wt%, and therefore the reaction rates are not hampered by the presence of pore-blocking EFW SnO_2 species. Moreover, as an increase in normalized STY is observed, the EFW species (site B type) must possess some catalytic activity. Indeed the STY of BV increases from 742 to 1202 h^{-1} with 1.6 and 3.6 wt% Sn, respectively, whereas UV analysis clearly indicated no additional formation of tetrahedral isolated Sn species (Site A types). A further comparison of the catalytic data with the UV features of the materials supports the idea that isolated Sn types (in site A) are very active for all reactions, and required to obtain activity in MPV and sugar isomerization. BV reactions can also be substantially catalyzed by oligomeric clusters (in site B). The seemingly independence of the DH/MPV rate for Sn loading (in the range of 0.5–8 wt%), despite a dropping accessibility of the tetrahedral Sn-sites in the pores of the material suggests that this reaction is also catalyzed by the EFW Sn species, albeit with a much lower catalytic efficiency. More likely, the reaction rate of DH/MPV should be taken with caution as DH rather than MPV is rate determining in the cascade reaction, as was discussed in an earlier publication [50].

3.3. Variation of Sn precursor

The identity of the Sn active site might change by varying the Sn-precursor during the grafting procedure. As explained above, $SnCl_4$ reacts with the silanol groups of the zeolite to form Sn—O—Si framework bonds, releasing HCl in the chemical process. A replacement of a Cl-atom of the Sn-precursor molecule with an alkyl group should easily prevent formation of such a framework bond. The alkyl groups are removed in a calcination step and likely result in SnOH formation. Note that the SnOH species, present in an 'open' Sn site, were proposed as an essential part of the active catalytic species in BV and MPV reactions [3,35]. Use of dibutyltin dichloride (Bu_2SnCl_2) onto MCM-41 was successfully tested [77], and more recently a dry impregnation of dimethyltin on dealuminated beta zeolite resulted in high concentrations of 'open' Sn sites and an elevated catalytic activity (in comparison with $SnCl_4$) in an epoxide hydration reaction [48].

Following the IPA grafting procedure, precursors with different alkyl groups, such as tetrabutyltin (Bu_4Sn^{IV}) (four alkyl groups), dibutyltin dichloride ($Bu_2Sn^{IV}Cl_2$), tin dichloride dihydrate ($Sn^{II}Cl_2{\cdot}2H_2O$) (two alkyl groups), tin tetrachloride pentahydrate ($Sn^{IV}Cl_4{\cdot}5H_2O$) and anhydrous $Sn^{IV}Cl_4$ were used. The elemental analysis (Table 3) shows a higher Sn-content for the final material for precursors with a higher number of Sn–Cl bonds, despite the use of equimolar concentrations of the precursor during its synthesis. This observation suggests that the driving force of the $SnCl_4$ adsorption is governed by the surface reaction between silanol and Sn–Cl. As significant amounts of Sn were found in IPA-graft with Bu_4Sn, also other adsorption pathways are present, presumably proceeding via adsorption onto the zeolite during the grafting procedure and disintegration of the molecule adsorbed species during the calcination step.

Metallic Sn powder, combined with an excess of 8 equivalents of HCl was also used as a precursor, by converting the metal *in situ* in the reflux solution to $SnCl_x$. This pathway was briefly explored due to the low cost of metallic Sn, but also to create a possible synthesis route to yield isotope enriched materials, in order to enhance the sensitivity of ^{119}Sn-characterization techniques like ^{119}Sn MAS NMR and ^{119}Sn Möβbauer. Interestingly, use of Sn^0/HCl in the IPA-graft procedure results in a higher Sn-content (Table 2), while no patches of undissolved Sn^0 or formed SnO_2 were found in the EPMA and X-ray diffraction analyses (Figs. S4 and S5).

Grafting of $SnCl_4{\cdot}5H_2O$, $SnCl_4$ and Bu_2SnCl_2 onto dealuminated beta zeolite all result in an intense UV absorption around 200 nm, indicative of pure tetrahedral $Sn^{IV}O_4$ moieties, recognized as the catalytically active Sn species (Fig. 5) [5]. Whereas this absorption is the single absorption feature for $SnCl_4{\cdot}5H_2O$, use of the other precursors leads to additional signals. For materials grafted with anhydrous $SnCl_4$ and Bu_2SnCl_2 precursors, these low UV energy absorption features are present at 263 nm and a shoulder at 245 nm (Fig. 5b and c). The observed absorptions are surprising, as formation of oligomeric or polymeric (hydrous) Sn oxides requires the presence of water molecules and no X-ray reflections of the oxide were found (Fig. S5). Residual Sn—Cl or Sn-alkylic may not be invoked since the first band shows UV absorption in the 120–210 nm range [78,79], while the latter Sn—C bond type is decomposed thorough calcination in air at high temperature [48,77]. However, it has to be noted that hydrothermally synthesized Snβ, believed to contain isolated tetrahedral Sn—O, also shows broad absorption features, with shoulders up to 300 nm [5,25,49,80]. Possibly, the secondary absorptive features are also related to isolated tetrahedral Sn-species, but showing different Sn—O bond lengths due to dissimilarities in the Sn geometry. The difference in nature and concentration of the Sn-species when using $SnCl_4{\cdot}5H_2O$ or its anhydrous equivalent is remarkable. Use of the former leads to a lower Sn loading, showing just one UV absorption feature, whereas in complete dry circumstances a higher Sn loading is obtained, showing multiple absorption signals. The difference in loading seems to be related to the strong interaction of the water molecules with the empty silanol nests in the dealuminated zeolite, as very strong interaction of water molecules with such silanols in zeolites has been proven with NMR and thermogravimetric analysis [81,82]. Occupation of the silanol nests with strongly bound water complicates reaction with $SnCl_4$, leading to lower Sn-loading.

$SnCl_2{\cdot}2H_2O$ and Bu_4 Sn-grafted materials show absorption maxima at 211 and 218 nm, respectively, and some secondary signals at 281 and 275–325 nm. The presence of Sn^{II} could be used to explain the 281 nm signal, though high temperatures in the presence of oxygen during the calcination ensures total oxidation to Sn^{IV} [51]. Weak signals of the d_{101} and d_{211} reflections of SnO_2

Please cite this article in press as: J. Dijkmans et al., Post-synthesis Snβ: An exploration of synthesis parameters and catalysis, J. Catal. (2015), http://dx.doi.org/10.1016/j.jcat.2015.06.023

Table 2
Comparison of the Sn-content and catalytic data of ISOM, MPV, BV and HS reactions for Sn-grafted catalyst synthesized with varying Sn precursors.

Entry	Precursor	Sn-content	ISOM		MPV		BV		DH/MPV	
			STY	TOF	STY	TOF	STY	TOF	STY	TOF
		wt%	h^{-1} (×1000)	h^{-1}	h^{-1} (×1000)	h^{-1}	h^{-1} (×1000)	h^{-1}	h^{-1} (×1000)	h^{-1}
1	$SnCl_4{\cdot}5H_2O$	1.6	3640	152	1277	96	741	49	1621	103
2	$SnCl_4$	2.9	2585	59	1143	47	495	17	1319	47
3[a]	$SnCl_4 + 5H_2O$	2.1	3100	97	1087	61	705	35	1274	61
4	Bu_2SnCl_2	0.8	2740	227	1154	174	633	87	1666	216
5	$SnCl_2{\cdot}2H_2O$	0.7	1233	112	933	140	578	83	198	28
6	Bu_4Sn	0.3	360	95	304	143	132	55	175	70
7	Sn^0/HCl[b]	2.6	2710	68	31	1.4	385	15	592	23

[a] Anhydrous $SnCl_4$ was mixed with 5 equivalents of water.
[b] Converted *in situ* to $SnCl_x$.

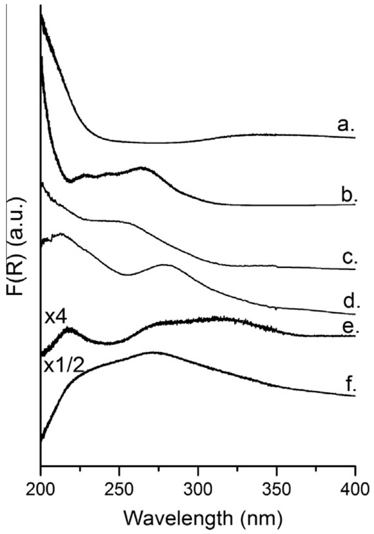

Fig. 5. DR-UV–vis spectra of material grafted with (a) $SnCl_4{\cdot}5H_2O$, (b) $SnCl_4$, (c) Bu_2SnCl_2, (d) $SnCl_2{\cdot}2H_2O$, (e) Bu_4Sn and (f) Sn^0/HCl. Samples were dried in N_2 at 823 K and corrected for dealuminated beta. Samples (e) and (f) are scaled with a factor of 4 and 0.5, respectively.

oxide were found in the X-ray diffraction pattern of the $SnCl_2$ grafted material (Fig. S4), indicative of a preferable a-selective deposition of Sn—O species. No such reflections were found for Bu_4Sn-grafted materials, possibly due to low Sn-content (below XRD bulk SnO_2 detection limit of 0.5 wt%, the low content also explains the low UV absorption intensity) or a more amorphous nature of the (hydrous) oxides. Whereas for $SnCl_2$, the secondary species can be assigned to polymeric Sn oxide species, for Bu_4Sn their nature is unclear. The high energy Sn—O species at about 200 nm are ascribed to tetrahedral Sn-species. Finally, the material grafted with a metallic Sn^0/HCl solution shows a broad absorption band between 200 and 400 nm with a maximum around 272 nm, whereas no Sn oxide related reflections were observed in X-ray analysis.

Use of Bu_2SnCl_2 instead of $SnCl_4$ was anticipated to generate more 'open' Sn sites. Since it has been reported that BV and ISOM reactions benefit from the presence of Sn—OH (or Si—OH), one could expect higher BV and ISOM activity of the Sn active sites of grafted Bu_2SnCl_2. Therefore, the presence of 'open' sites was evaluated by a reported FTIR study, using deuterated acetonitrile [4]. Absorption bands at 2308 and 2316 cm^{-1} were assigned to acetonitrile ($\nu C{\equiv}N$) adsorbed on 'closed' and 'open' Sn sites, respectively. The spectra of $SnCl_4{\cdot}5H_2O$ and Bu_2SnCl_2 are shown in Fig. 6(1). The signal at 2274 cm^{-1} is due to acetonitrile interacting with silanol groups. Interestingly, since both materials show an absorption feature at 2308 cm^{-1}, predominantly 'closed' Sn sites are expected to be present in both samples.

A similar FTIR experiment was performed with cyclohexanone instead of acetonitrile. Here, the vibration frequency of the carbonyl group was taken as a measure of the Lewis acid strength: the larger the wavenumber, the stronger the Lewis acid interaction. The data of two Snβ catalysts, grafted with Bu_2SnCl_2 and $SnCl_4$, are presented in Fig. 6(2). The vibration of an unperturbed carbonyl group, likely of physisorbed cyclohexanone, is visible at 1714 cm^{-1}. Upon adsorption on Sn this vibration shifts to higher frequencies. As both $SnCl_4$ and Bu_2SnCl_2 grafted materials show a similar shift of the carbonyl vibration to 1652 cm^{-1} (at 423 K), it is concluded that the Lewis acidity of both Sn-sites is similar. This statement is also confirmed by a temperature programmed FTIR study with pyridine, the data being presented in Fig. 6(3). The ratio of pyridine sorbed onto the Lewis acid sites of both materials at 523 compared to 423 K is very similar, *viz.* 0.22 for $SnCl_4$-grafted materials and 0.24 for Bu_2SnCl_2 grafted materials, confirming that the Sn-sites have very similar Lewis acid strengths. The lower intensity of the signal for the Bu_2SnCl_2 grafted material points to lower concentration of adsorbed pyridine, in line with its lower Sn-content. A similar trend is visible in the deuterated acetonitrile and cyclohexanone probed spectra.

In conclusion, although the nature of the Sn-species in the various materials may not be fully established by the characterization techniques, it is clear that use of different Sn-precursors results in varying Sn-species in the final Sn beta zeolites. However, irrespective of the differences in the electronic spectra, Sn sites with different electronic properties may deliver comparable Lewis acid properties, and therefore may lead to comparable catalytic results.

The catalytic data for the different reactions tested in terms of TOF and STY values, are summarized in Table 2. For all reaction types, the precursor Bu_2SnCl_2 showed the highest activity per Sn atom, though the activity order depends on the reaction type. The TOF-ranking for ISOM is $Bu_2SnCl_2 > SnCl_4{\cdot}5H_2O > SnCl_2 > Bu_4Sn > Sn^0/HCl = SnCl_4$, while for MPV it is $Bu_2SnCl_2 > SnCl_2 = Bu_4Sn > SnCl_4{\cdot}5H_2O > SnCl_4 > Sn^0/HCl$; for BV it is $Bu_2SnCl_2 = SnCl_2 > Bu_4Sn = SnCl_4{\cdot}5H_2O > SnCl_4 > Sn^0/HCl$ and for DH/MPV: $Bu_2SnCl_2 \gg SnCl_4{\cdot}5H_2O > Bu_4Sn > SnCl_4 > SnCl_2 > Sn^0/HCl$. Therefore, it seems that the occurrence of Sn after grafting with Bu_2SnCl_2 provides suitable active sites, whereas different, less active sites are present on the other catalysts. Nevertheless, these sites show diverse activity depending on the reaction type.

As in previous paragraphs the negative impact of Sn loading on activity for a specific Sn precursor, *viz.* $SnCl_4{\cdot}5H_2O$, was demonstrated, STY values should preferably be plotted against Sn loading in order to judge the catalytic performance (Fig. 6). By filtering out the Sn loading effect, ISOM catalysis best proceeds with the $SnCl_4{\cdot}5H_2O$-grafted materials, irrespective of the Sn loading (Fig. 7a). The catalyst is most productive with a Sn loading below

Please cite this article in press as: J. Dijkmans et al., Post-synthesis Snβ: An exploration of synthesis parameters and catalysis, J. Catal. (2015), http://dx.doi.org/10.1016/j.jcat.2015.06.023

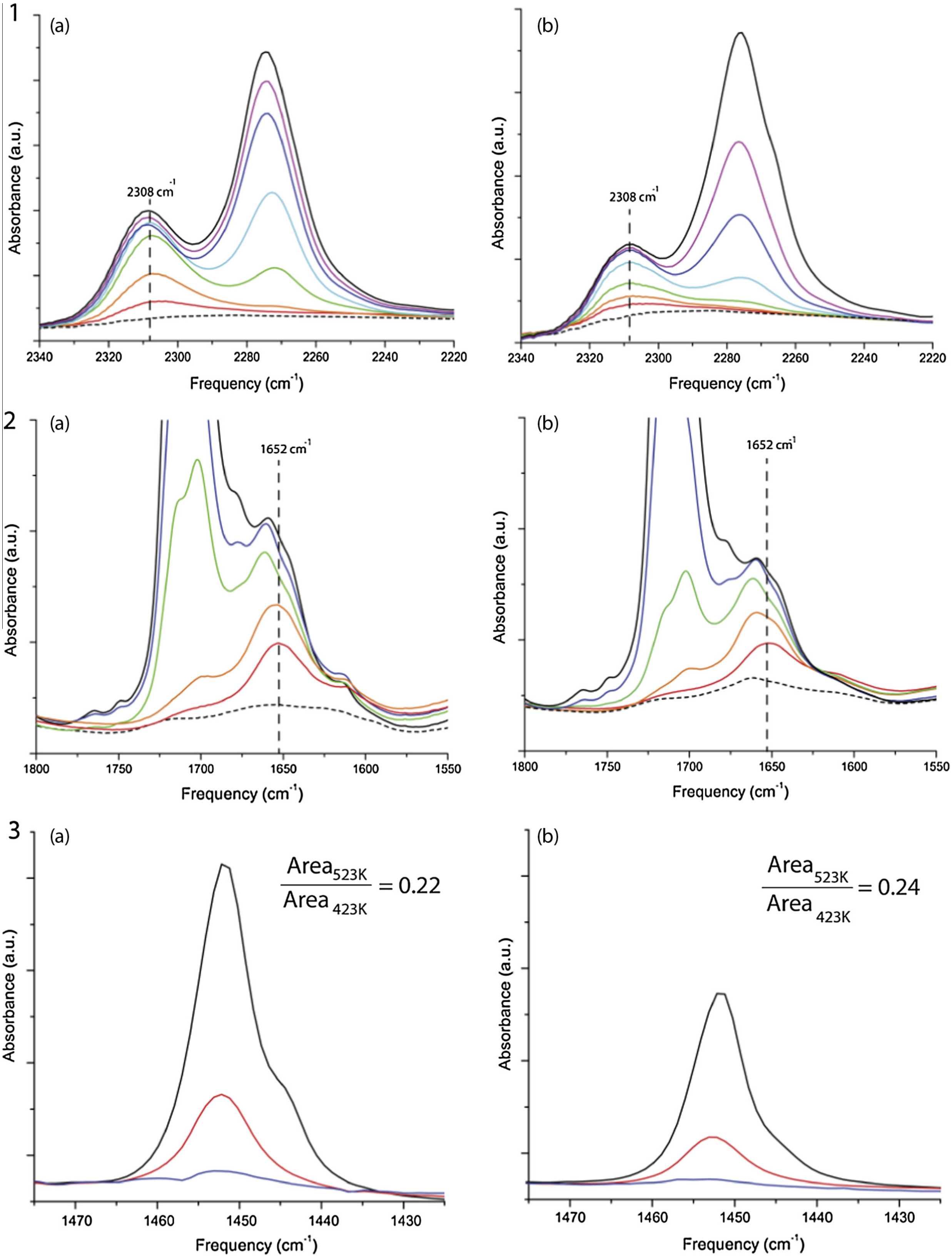

Fig. 6. (1) FTIR of deuterated acetonitrile desorbing of (a) $SnCl_4{\cdot}5H_2O$ grafted, (b) Bu_2SnCl_2 grafted dealuminated beta zeolite. The black dotted line shows the main signal of acetonitrile adsorbed onto Lewis acid sites. (2) FTIR of cyclohexanone desorbing of (a) $SnCl_4$-grafted, (b) Bu_2SnCl_2-grafted dealuminated beta zeolite. The black dotted line shows the main signal of cyclohexanone adsorbed onto Lewis acid sites. (3) FTIR spectrum of adsorbed pyridine on (a) $SnCl_4$-grafted, (b) Bu_2SnCl_2-grafted, dealuminated beta zeolite. Desorption of the probe molecule at 423 K (black), 523 K (red) and 623 K (blue) was investigated. Samples were evacuated before measurement and signals are scaled to weight. Ratios of the surface area of the Lewis acid adsorbed pyridine vibration around 1451 cm^{-1} are given for 523 *vs.* 423 K. (For interpretation of the references to color in this figure legend, the reader is referred to the web version of this article.)

1 wt%, likely because of the requirement of very specific Sn isolated tetrahedral sites with UV absorption features below 210 nm.

In case of MPV (Fig. 7b), STY shows independent behavior of the precursor type, except for Sn^0/HCl. Merely the Sn loading is the determining factor for productivity, showing the most productive material with a Sn loading of about 2 wt%. MPV therefore requires preferably tetrahedral Sn sites with absorption features below 210 nm, which are less specific than those for ISOM. Clearly, the Sn species formed by grafting in Sn^0/HCl are undesired for MPV. The low activity of this catalyst, containing many oligomeric Sn—O species and no isolated tetrahedral Sn—O, emphasizes the importance of the isolated Sn species for catalytic MPV activity.

A similar trend is observed for BV (Fig. 7c). The relationship of STY with Sn loading is similar for most Sn precursors, except for the anhydrous $SnCl_4$ and Sn^0/HCl. The Sn loading for maximum STY values though is clearly higher, corresponding to 4 wt%. Such high value reveals that oligomeric Sn species also exhibit considerable BV activity, whereas their activity is very low for ISOM and MPV. The underperformance of $SnCl_4$ and Sn^0/HCl demonstrates specific electronic and geometric requirements of the oligomeric active sites, though their nature is unclear at this stage.

Finally, the productivity of the catalysts was compared for DH/MPV in Fig. 7d. This reaction type clearly prefers the catalyst obtained from the $SnCl_4{\cdot}5H_2O$ or Bu_2SnCl_2 precursor. The STY is independent of the Sn concentration, indicating that the cascade reaction probably needs a Sn in a reaction step that is not rate determining. Literature describes that the dehydration, preferably carried out with (mild) Brønsted acidity for instance originating as a result of Sn grafting [83], the presence of Al^{3+}-sites [50] or oxygen containing carbon groups [17], determines the rate, whereas the Sn-catalyzed hydride-shift is not. Although unclear now, the underperformance of the other catalysts should therefore be caused by a deficit of Brønsted acidity on the final catalyst.

The difference between a $SnCl_4{\cdot}5H_2O$ precursor and its anhydrous counterpart was investigated by carrying out a synthesis, in which 5 molar equivalents of water were added to the anhydrous precursor. An increase in Sn-content but a lower catalytic performance were found for this material (Entry 3 in Table 2 and Fig. 7) in comparison with those made with the hydrated $SnCl_4{\cdot}5H_2O$ salt. This result suggests that (crystal) water plays an important role in the grafting procedure (*vide infra*), which cannot be simply replaced by free water molecules.

3.4. Effect of water concentration during the Sn grafting step

Finally, the influence of water on the grafting of Sn was investigated. Assuming water may react with $SnCl_4$, producing (hydrous) oxide complexes of Sn and HCl already in the reflux isopropanol solution, deposition of oligomeric EFW Sn oxide patches may be expected when the water content is too high. In fact, the formation of large Sn oxide phases were indeed observed by grafting with an aqueous $SnCl_4$ solution (*vide supra*, section on synthesis method exploration). To understand the consequence of the water effect on Sn catalysis, grafting in isopropanol was investigated in the presence of varying amounts of water. Therefore, the dealuminated zeolite powder was activated at 423 K under dry air to remove

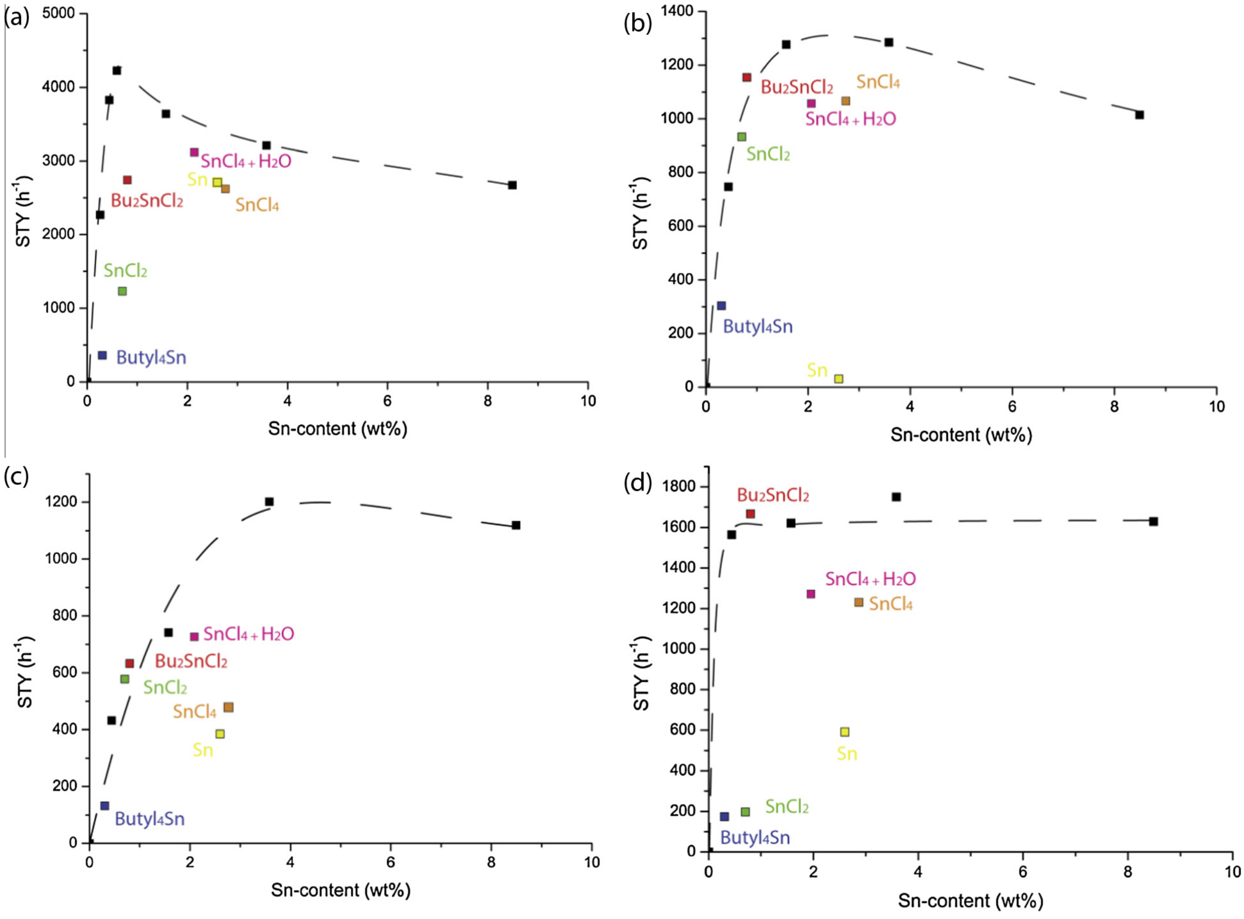

Fig. 7. STY (×1000) in function of Sn loading for (a) ISOM, (b) MPV, (c) BV, and (d) DH/MPV reactions catalyzed by samples synthesized with changing Sn-precursor. The black data points are from $SnCl_4{\cdot}5H_2O$, orange is anhydrous $SnCl_4$, pink is mixture of anhydrous $SnCl_4$ and 5 equivalents of water, red is $Butyl_2SnCl_2$, green is $SnCl_2$, blue is $Butyl_4Sn$ and yellow is metallic Sn. The black lines are guides to the eye and indicates the trend for $SnCl_4{\cdot}5H_2O$. (For interpretation of the references to color in this figure legend, the reader is referred to the web version of this article.)

Please cite this article in press as: J. Dijkmans et al., Post-synthesis Snβ: An exploration of synthesis parameters and catalysis, J. Catal. (2015), http://dx.doi.org/10.1016/j.jcat.2015.06.023

physisorbed water before being added to dry isopropanol. Known aliquots of water were then added to the grafting solution containing a constant concentration of $SnCl_4 \cdot 5H_2O$. Elemental analysis of obtained Snβ samples is presented in Table 3.

The presence of some water results in a higher Sn adsorption. Whereas a Sn loading of 1.6 wt% was found for water to Sn molar ratio of 5, further increase this ratio leads to higher Sn loadings; *e.g.*, 3.8 and 11.3 wt% of Sn for a ratio of 6.5 and 31, respectively. High water contents generate oligomeric (hydrous) oxide forms of Sn as a result of Sn chloride salt hydrolysis, leading to nonselective adsorption in and on the zeolite crystals. Their formation is clearly apparent in the XRD patterns, presented in Fig. 2(f), though finely dispersed and invisible in SEM electrographs (Fig. S6). Ultimately, at very high water contents or grafting in pure water, separate Sn (hydrous) oxide phases are formed next to the zeolite crystals, as indicated by micrographs and EPMA analysis (Fig. S1).

The samples were also investigated with UV–vis DR spectroscopy. Clearly, the low energy absorption band in the electronic spectrum shifts to higher wavelengths for Snβ samples prepared in reflux solution with higher water content (Fig. 8). This shift indeed points to the presence of larger Sn (hydrous) EFW oxide phases with increasing water content in the reflux solution.

A FTIR spectroscopic analysis of the silanol groups of a material grafted in the presence of a high concentration of water (H_2O:Sn = 31) shows only a slight drop in the concentration of the internal silanols, whereas the external silanol groups remain unchanged (data in Table S3). Though this trend is similar to samples grafted in the presence of low water concentration, the absolute decrease of internal silanols is considerably less outspoken. Nevertheless, the UV-absorption of the 200 nm signal, which was assigned to Sn-species adsorbed in the internal silanol nests, of the materials synthesized in the presence of water is similar to this of materials made in water-limiting conditions, suggesting equal amounts of such tetrahedral type A Sn-species. Possibly, the presence of water generates additional silanol groups during the grafting process, e.g., by siloxane hydration or additional dealumination. Analysis of the micropore volume and the Lewis acidity of materials prepared in high water to Sn molar ratios by N_2-sorption and pyridine probed FTIR respectively, suggests a significant decrease in Sn accessibility. For instance, a significant decrease in micropore volume, *viz.* from 0.16 to 0.05 ml g^{-1} for materials grafted with H_2O:Sn of 5 and 31 respectively was measured, while the total Lewis acidity probed per Sn-atom decreased from 0.7 to 0.2 (data in Table S3). These observations point to a serious pore blockage by the present EFW SnO_2 species.

^{119}Sn MAS NMR of a sample prepared with a high H_2O:Sn ratio of 12 was measured. The spectrum (Fig. S7) only shows a broad feature at −715 ppm, a diagnostic chemical shift of tetrahedrally coordinated Sn, whereas a signal at −604 ppm of polymeric octahedrally coordinated Sn, like in bulk SnO_2, is absent, despite clear presence of the EFW Sn species from UV absorption. A similar analysis with bulk SnO_2 in beta zeolites shows a clear −604 ppm signal after a short measuring time (Fig. S8). Therefore, the 280 nm Sn oxide species is tentatively assigned to oligomeric tetrahedral Sn sites. Unfortunately, as NMR spectroscopy of oxidic Sn species is not as mature as NMR of other more abundant nuclei like Al and Si, any assignment should be considered with caution. Indeed, there are reports pointing to signal intensity reduction and broadening of nano-sized oligomeric Sn oxides [84,85]. Improving ^{119}Sn MAS NMR resolution and better identification of chemical shifts is currently under research using ^{119}Sn enriched samples or by using Dynamic Nuclear Polarization NMR techniques [51,86].

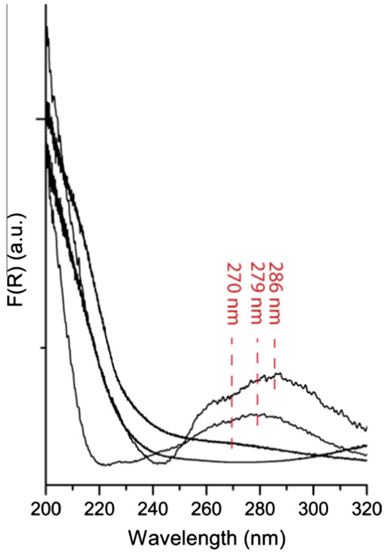

Fig. 8. UV-spectrum of samples synthesized with H_2O:Sn-ratio of 5, 6.5, 12 and 31 (bottom to top at 280 nm). The secondary Sn-species maxima are labeled. Samples were dried in N_2 at 823 K and corrected for dealuminated beta.

The different Snβ catalysts were tested in the four reactions (Table 3 and Fig. S9). As before, the highest TOFs for each reaction type were found for the lowest Sn contents. In contrast to previous catalytic tests with increasing Sn loadings (by increasing $SnCl_4 \cdot 5H_2O$ concentration in the reflux), the higher Sn loadings do not lead to higher STYs. Obviously, the abundant presence of oligomeric EFW Sn species blocks the pore entrance, as evidenced by the micropore volume decrease, leading to a loss of catalyst efficiency. This suggests that the Sn speciation is different, and thus not only depends on the Sn content, but also on other grafting parameters like the water content in the reflux solution. The best catalysis both in terms of TOF and STY was achieved when Snβ is made by Sn adsorption in dry isopropanol with water to Sn molar ratio of 5.

4. Conclusions

Contacting a Sn precursor with a dealuminated zeolite is a practical synthesis method to produce Sn containing Beta catalysts, which are active in four different Lewis acid catalyzed reaction types (ISOM, MPV, BV and DH/MPV). The occurrence of Sn is highly

Table 3
Comparison of the Sn-content and catalytic data of ISOM, MPV, BV and HS reaction for Sn-grafted catalyst synthesized in the presence of varying H_2O:Sn-ratio.

Entry	H_2O:Sn	Sn-content	ISOM		MPV		BV		DH/MPV	
		wt%	STY h^{-1} (×1000)	TOF h^{-1}	STY h^{-1} (×1000)	TOF h^{-1}	STY h^{-1} (×1000)	TOF h^{-1}	STY h^{-1} (×1000)	TOF h^{-1}
1	5	1.6	3640	152	1277	96	714	47	1621	103
2	6.5	3.8	2556	44	1021	32	473	13	1370	36
3	12	7.1	2098	19	303	5	401	6	1187	17
4	31	11.3	1496	9	173	2	274	3	935	8

Please cite this article in press as: J. Dijkmans et al., Post-synthesis Snβ: An exploration of synthesis parameters and catalysis, J. Catal. (2015), http://dx.doi.org/10.1016/j.jcat.2015.06.023

dependent on the Sn introduction method (solid mix, impregnation, sorption) and on synthesis parameters like Sn precursor, precursor and water concentration during the contact process. Likely, though several methods may lead to active Snβ catalysts, they require different protocols to introduce the most active Sn sites. This contribution elaborated on the sorption method in liquid, that is grafting a Sn precursor into the silanol nests of the dealuminated Beta zeolite. Two different sorption sites were observed: one site-selective sorption in the internal silanol nests (site A), taking place below 2 wt% Sn loading and creating isolated Sn sites, and one a-selective sorption above 2 wt% of Sn, leading to oligomeric EFW Sn species (site B), both sites showing low affinity for the Sn precursor. To increase the affinity of the silanol site, removal of water from the adsorption site and use of Sn precursor with considerable chloride ligands are advised.

Efforts were carried out to clarify the identity of the two Sn sites using various spectroscopic tools. The isolated Sn sites are tetrahedral in coordination in line with its absorption feature below 200 nm in the electronic spectrum. Higher Sn loadings showed formation of oligomeric EFW species, usually with UV absorption at about 255 nm, but also at higher wavelengths (280 nm) in case of the presence of high concentrations of water in the grafting solution. Shoulders up to 300 nm were observed when the Sn loading is above 10 wt%. The presence of the latter is often accompanied with small X-ray reflections of SnO_2 in the diffractogram, suggesting they are octahedrally coordinated and polymerized Sn—O like in bulk SnO_2, and a phase separation observable in EPMA/SEM graphs. It is difficult to distinguish Sn—O species absorbing at intermediate UV wavelengths. Based on ^{119}Sn MAS NMR, the 280 nm Sn species and therefore the 255 nm is also tentatively considered in tetrahedral coordination. Though its nuclearity is assumed to be oligomeric, the 255 nm feature may also result from tetrahedral species with one or multiple extended Sn—O bonds.

Catalytic performance may be expressed as turn-over frequency and space-time-yield. While the first measures the activity per Sn active site, assuming every Sn is accessible, the second one refers to the activity per catalyst weight. Whereas general agreement exists that isolated Sn sites have to be correlated to the most active Lewis acid sites, the other Sn species also contribute to Lewis acid catalyzed reactions, depending on the reaction type. Increase of Sn loading may therefore improve the productivity of the catalysis, albeit not linearly correlated to the Sn loading. Since site requirements are most specific for the aldo/keto isomerization of sugars and Meerwein–Ponndorf–Verley, an increase of Sn loading by grafting is not very helpful to increase product formation as at high Sn-loadings, formation of inactive EFW species occurs, which additionally cause pore blockage. High productivity will therefore only be achieved by searching for new synthetic methods, accounting for high densities of framework tetrahedral Sn active sites. However, oligomeric EFW species show considerable catalytic contribution in the BV reaction. This reaction type therefore benefits from increasing Sn loadings, despite a constant lowering of activity per Sn site. Too high Sn loadings by grafting though should be avoided because of pore blocking, resulting into decreasing STYs. Conclusions on the cascade reaction (DH/MPV) should be taken with caution, as this test reaction preferably requires Brønsted acid sites in the rate determining dehydration step.

Acknowledgments

Prof. Bart Blanpain is gratefully thanked for the EPMA measurements Hercules Foundation (project ZW09-09) is acknowledged for the funding of the JEOL JXA-8530F EPMA. IOF-KP/14/003 is thanked for financial support of the authors.

Appendix A. Supplementary material

Supplementary data associated with this article can be found, in the online version, at http://dx.doi.org/10.1016/j.jcat.2015.06.023.

References

[1] Y. Román-Leshkov, M.E. Davis, ACS Catal. 1 (2011) 1566.
[2] M. Moliner, Dalton Trans. 43 (2014) 4197.
[3] M. Boronat, A. Corma, M. Renz, J. Phys. Chem. B 110 (2006) 21168.
[4] M. Boronat, P. Concepcion, A. Corma, M. Renz, S. Valencia, J. Catal. 234 (2005) 111.
[5] R. Bermejo-Deval, R. Gounder, M.E. Davis, ACS Catal. 2 (2012) 2705.
[6] M. Dusselier, P. Van|Wouwe, F. de|Clippel, J. Dijkmans, D.W. Gammon, B.F. Sels, ChemCatChem 5 (2013) 569.
[7] Y. Hayashi, Y. Sasaki, Chem. Commun. (2005) 2716.
[8] M. Dusselier, P. Van Wouwe, S. De Smet, R. De Clercq, L. Verbelen, P. Van Puyvelde, F.E. Du Prez, B.F. Sels, ACS Catal. 3 (2013) 1786.
[9] S. Yamaguchi, K. Motokura, Y. Sakamoto, A. Miyaji, T. Baba, Chem. Commun. 50 (2014) 4600.
[10] S. Yamaguchi, T. Matsuo, K. Motokura, Y. Sakamoto, A. Miyaji, T. Baba, ChemSusChem 8 (2015) 853.
[11] G. Tian, X. Tong, Y. Cheng, S. Xue, Carbohydr. Res. 370 (2013) 33.
[12] L. Zhou, L. Wu, H. Li, X. Yang, Y. Su, T. Lu, J. Xu, J. Mol. Catal. A: Chem. 388–389 (2014) 74.
[13] J. Venselaar, Gas-Phase Aldol Condensation over Tin on Silica Catalysts, Delft University, Delft, 1980. pp. 140.
[14] L. Li, X. Collard, A. Bertrand, B.F. Sels, P.P. Pescarmona, C. Aprile, J. Catal. 314 (2014) 56.
[15] M. Saito, H. Ikeda, Y. Horiuchi, M. Matsuoka, Res. Chem. Intermed. 40 (2014) 87.
[16] A.L. Villa, L.F. Correa, E.A. Alarcón, Chem. Eng. J. 215–216 (2013) 500.
[17] F. de Clippel, M. Dusselier, R. Van Rompaey, P. Vanelderen, J. Dijkmans, E. Makshina, L. Giebeler, S. Oswald, G.V. Baron, J.F.M. Denayer, P.P. Pescarmona, P.A. Jacobs, B.F. Sels, J. Am. Chem. Soc. 134 (2012) 10089.
[18] C.M. Osmundsen, M.S. Holm, S. Dahl, E. Taarning, Proc. Roy. Soc. A 468 (2012) 2000.
[19] S. Sisodiya, S. Shylesh, A.P. Singh, Catal. Commun. 12 (2011) 629.
[20] A.C. Garade, P.S. Niphadkar, P.N. Joshi, C.V. Rode, Chem. Lett. 39 (2010) 126.
[21] U.S. Taralkar, P. Kalita, R. Kumar, P.N. Joshi, Appl. Catal. A 358 (2009) 88.
[22] S. Endud, K.-L. Wong, Microporous Mesoporous Mater. 101 (2007) 256.
[23] A. Corma, M. Renz, Collect. Czech. Chem. Commun. 70 (2005) 1727.
[24] A.L. Villa de P, E. Alarcon, C. Montes de Correa, Chem. Commun. (2002) 2654.
[25] A. Corma, L.T. Nemeth, M. Renz, S. Valencia, Nature 412 (2001) 423.
[26] N.K. Mal, A. Bhaumik, R. Kumar, A.V. Ramaswamy, Catal. Lett. 33 (1995) 387.
[27] N.K. Mal, A. Bhaumik, V. Ramaswamy, A.A. Belhekar, A.V. Ramaswamy, in: H.K. Beyer, H.G. Karge, I. Kiricsi, J.B. Nagy (Eds.), Stud. Surf. Sci. Catal, Elsevier, Amsterdam, 1995, p. 317.
[28] N.K. Mal, V. Ramaswamy, S. Ganapathy, A.V. Ramaswamy, J. Chem. Soc. Chem. Commun. (1994) 1933.
[29] H.Y. Luo, L. Bui, W.R. Gunther, E. Min, Y. Román-Leshkov, ACS Catal. 2 (2012) 2695.
[30] E. Taarning, S. Saravanamurugan, M.S. Holm, J. Xiong, R.M. West, C.H. Christensen, ChemSusChem 2 (2009) 625.
[31] S. Tolborg, A. Katerinopoulou, D.D. Falcone, I. Sadaba, C.M. Osmundsen, R.J. Davis, E. Taarning, P. Fristrup, M.S. Holm, J. Mater. Chem. A 2 (2014) 20252.
[32] S.V. Valencia, A.C. Corma, US005968473A, 1999, to UOP.
[33] A. Corma, M.E. Domine, S. Valencia, J. Catal. 215 (2003) 294.
[34] S. Van de Vyver, C. Odermatt, K. Romero, T. Prasomsri, Y. Roman-Leshkov, ACS Catal. (2015).
[35] M. Boronat, A. Corma, M. Renz, G. Sastre, P.M. Viruela, Chem. A Euro. J. 11 (2005) 6905.
[36] G. Li, E.A. Pidko, E.J.M. Hensen, Catal. Sci. Technol. (2014).
[37] G. Yang, E.A. Pidko, E.J.M. Hensen, ChemSusChem (2013).
[38] R. van Grieken, C. Martos, M. Sánchez-Sánchez, D.P. Serrano, J.A. Melero, J. Iglesias, A.G. Cubero, Microporous Mesoporous Mater. 119 (2009) 176.
[39] C.-C. Chang, Z. Wang, P. Dornath, H. Je Cho, W. Fan, RSC Adv. (2012).
[40] Z. Kang, X. Zhang, H. Liu, J. Qiu, K.L. Yeung, Chem. Eng. J. 218 (2013) 425.
[41] A. Omegna, M. Vasic, J. Anton van Bokhoven, G. Pirngruber, R. Prins, Phys. Chem. Chem. Phys. 6 (2004) 447.
[42] J.A. van Bokhoven, D.C. Koningsberger, P. Kunkeler, H. van Bekkum, A.P.M. Kentgens, J. Am. Chem. Soc. 122 (2000) 12842.
[43] Q. Guo, F. Fan, E.A. Pidko, W.N.P. van der Graaff, Z. Feng, C. Li, E.J.M. Hensen, ChemSusChem 6 (2013) 1352.
[44] P.Y. Dapsens, C. Mondelli, J. Jagielski, R. Hauert, J. Perez-Ramirez, Catal. Sci. Technol. 4 (2014) 2302.
[45] P. Li, G. Liu, H. Wu, Y. Liu, J.-G. Jiang, P. Wu, J. Phys. Chem. C 115 (2011) 3663.
[46] W.N.P. van der Graaff, G. Li, B. Mezari, E.A. Pidko, E.J.M. Hensen, ChemCatChem (2015). n/a.
[47] C. Hammond, S. Conrad, I. Hermans, Angew. Chem. Int. Edit. 51 (2012) 11736.
[48] B. Tang, W. Dai, G. Wu, N. Guan, L. Li, M. Hunger, ACS Catal. 4 (2014) 2801.
[49] J. Dijkmans, D. Gabriels, M. Dusselier, F. de Clippel, P. Vanelderen, K. Houthoofd, A. Malfliet, Y. Pontikes, B.F. Sels, Green Chem. 15 (2013) 2777.

Please cite this article in press as: J. Dijkmans et al., Post-synthesis Snβ: An exploration of synthesis parameters and catalysis, J. Catal. (2015), http://dx.doi.org/10.1016/j.jcat.2015.06.023

[50] J. Dijkmans, D. Gabriëls, M. Dusselier, K. Houthoofd, P.C.M.M. Magusin, S. Huang, Y. Pontikes, M. Trekels, A. Vantomme, L. Giebeler, S. Oswald, B.F. Sels, ACS Catal. 5 (2015) 928.

[51] P. Wolf, M. Valla, A.J. Rossini, A. Comas-Vives, F. Núñez-Zarur, B. Malaman, A. Lesage, L. Emsley, C. Copéret, I. Hermans, Angew. Chem. Int. Ed. 53 (2014) 10179.

[52] M. Moliner, Y. Román-Leshkov, M.E. Davis, Proc. Natl. Acad. Sci. U. S. A. 107 (2010) 6164.

[53] M.T. Musser, Ullmann's Encyclopedia of Industrial Chemistry, Wiley-VCH Verlag GmbH & Co. KGaA, 2000.

[54] J. Ritz, H. Fuchs, H. Kieczka, W.C. Moran, Ullmann's Encyclopedia of Industrial Chemistry, Wiley-VCH Verlag GmbH & Co. KGaA, 2000.

[55] M. Dusselier, P. Van Wouwe, A. Dewaele, P.A. Jacobs, B.F. Sels, Science 349 (2015) 78.

[56] G. Ertl, H. Knözinger, F. Schüth, J. Weitkamp, Handbook of Heterogeneous Catalysis: Preparation of Solid Catalysts, Wiley-VCH, 2008.

[57] Z. Kang, H.o. Liu, X. Zhang, Chin. J. Catal. 33 (2012) 898.

[58] M. Casagrande, E. Moretti, L. Storaro, M. Lenarda, J. Gersich, L. Stievano, F.E. Wagner, Microporous Mesoporous Mater. 91 (2006) 261.

[59] L. Haiou, K. Zihua, Z. Xiongfu, Q. Jie-shan, CN102249258 A, 2011, to D.U.o. Technology.

[60] N.S. Nesterenko, F. Thibault-Starzyk, V. Montouilliout, V.V. Yushchenko, C. Fernandez, J.P. Gilson, F. Fajula, I.I. Ivanova, Kinet. Catal. 47 (2006) 40.

[61] K. Chaudhari, T.K. Das, P.R. Rajmohanan, K. Lazar, S. Sivasanker, A.J. Chandwadkar, J. Catal. 183 (1999) 281.

[62] M.D. González, Y. Cesteros, P. Salagre, Microporous Mesoporous Mater. 144 (2011) 162.

[63] E.B. Lami, F. Fajula, D. Anglerot, T. Des Courieres, Microporous Mater. 1 (1993) 237.

[64] J.P. Marques, I. Gener, P. Ayrault, J.C. Bordado, J.M. Lopes, F. Ramôa Ribeiro, M. Guisnet, Microporous Mesoporous Mater. 60 (2003) 251.

[65] D.M. Roberge, H. Hausmann, W.F. Holderich, Phys. Chem. Chem. Phys. 4 (2002) 3128.

[66] T. Witvrouwen, J. Dijkmans, S. Paulussen, B. Sels, J. Energy Chem. 22 (2013) 451.

[67] Z. Chen, J.K.L. Lai, C.H. Shek, H. Chen, J. Mater. Res. 18 (2003).

[68] O. Lupan, L. Chow, G. Chai, H. Heinrich, S. Park, A. Schulte, J. Cryst. Growth 311 (2008) 152.

[69] G. Pang, S. Chen, Y. Koltypin, A. Zaban, S. Feng, A. Gedanken, Nano Lett. 1 (2001) 723.

[70] H.S. Taylor, Proc. Roy. Soc. A 108 (1925) 355.

[71] B. Peters, S.L. Scott, J. Chem. Phys. 142 (2015) 104708.

[72] R.E. Parales, K. Lee, S.M. Resnick, H. Jiang, D.J. Lessner, D.T. Gibson, J. Bacteriol. 182 (2000) 1641.

[73] A. Fürstner, L. Ackermann, B. Gabor, R. Goddard, C.W. Lehmann, R. Mynott, F. Stelzer, O.R. Thiel, Chem. Euro. J. 7 (2001) 3236.

[74] C.A. Emeis, J. Catal. 141 (1993) 347.

[75] A. Vimont, F. Thibault-Starzyk, J.C. Lavalley, J. Phys. Chem. B 104 (1999) 286.

[76] S. Khabtou, T. Chevreau, J.C. Lavalley, Microporous Mater. 3 (1994) 133.

[77] A. Corma, M.T. Navarro, M. Renz, J. Catal. 219 (2003) 242.

[78] J. Fernandez, G. Lespes, A. Dargelos, Chem. Phys. 111 (1987) 97.

[79] M. Rothschild, Laser Microfabrication: Thin Film Processes and Lithography, Elsevier, 1989.

[80] S.R. Bare, S.D. Kelly, W. Sinkler, J.J. Low, F.S. Modica, S. Valencia, A. Corma, L.T. Nemeth, J. Am. Chem. Soc. 127 (2005) 12924.

[81] J. Van Aelst, M. Haouas, E. Gobechiya, K. Houthoofd, A. Philippaerts, S.P. Sree, C.E.A. Kirschhock, P. Jacobs, J.A. Martens, B.F. Sels, F. Taulelle, J. Phys. Chem. C 118 (2014) 22573.

[82] E. Verheyen, L. Joos, C. Martineau, C.J. Dawson, C. Weidenthaler, W. Schmidt, R. Yuan, E. Breynaert, V. Van Speybroeck, M. Waroquier, F. Taulelle, M.M.J. Treacy, J.A. Martens, C.E.A. Kirschhock, Mater. Horizons 1 (2014) 582.

[83] L. Li, C. Stroobants, K. Lin, P.A. Jacobs, B.F. Sels, P.P. Pescarmona, Green Chem. 13 (2011) 1175.

[84] T. Dey, P. Khuntia, A.V. Mahajan, Europhys. Lett. 96 (2011) 670081.

[85] D.P. Tunstall, S. Patou, R.S. Liu, Y.H. Kao, Mater. Res. Bull. 34 (1999) 1513.

[86] W.R. Gunther, V.K. Michaelis, M.A. Caporini, R.G. Griffin, Y. Román-Leshkov, J. Am. Chem. Soc. 136 (2014) 6219.

Please cite this article in press as: J. Dijkmans et al., Post-synthesis Snβ: An exploration of synthesis parameters and catalysis, J. Catal. (2015), http://dx.doi.org/10.1016/j.jcat.2015.06.023